frontiers | Frontiers in Immunology

TYPE Original Research
PUBLISHED 26 March 2024
DOI 10.3389/fimmu.2024.1370511

OPEN ACCESS

EDITED BY
Brian J. Ferguson,
University of Cambridge, United Kingdom

REVIEWED BY
Uday Kishore,
United Arab Emirates University, United Arab Emirates
Jinghua Lu,
National Institute of Allergy and Infectious Diseases (NIH), United States

*CORRESPONDENCE
Guirong Wang
wangg@upstate.edu

RECEIVED 14 January 2024
ACCEPTED 11 March 2024
PUBLISHED 26 March 2024

CITATION
Jacob IB, Gemmiti A, Xiong W, Reynolds E, Nicholas B, Thangamani S, Jia H and Wang G (2024) Human surfactant protein A inhibits SARS-CoV-2 infectivity and alleviates lung injury in a mouse infection model. *Front. Immunol.* 15:1370511. doi: 10.3389/fimmu.2024.1370511

Human surfactant protein A inhibits SARS-CoV-2 infectivity and alleviates lung injury in a mouse infection model

Ikechukwu B. Jacob[1,2], Amanda Gemmiti[3], Weichuan Xiong[1], Erin Reynolds[2], Brian Nicholas[3], Saravanan Thangamani[2], Hongpeng Jia[4] and Guirong Wang[1,2*]

[1]Department of Surgery, the State University of New York (SUNY) Upstate Medical University, Syracuse, NY, United States, [2]Department of Microbiology & Immunology, SUNY Upstate Medical University, Syracuse, NY, United States, [3]Department of Otolaryngology, SUNY Upstate Medical University, Syracuse, NY, United States, [4]Department of Surgery, Johns-Hopkins University, Baltimore, MD, United States

Introduction: SARS coronavirus 2 (SARS-CoV-2) infects human angiotensin-converting enzyme 2 (hACE2)-expressing lung epithelial cells through its spike (S) protein. The S protein is highly glycosylated and could be a target for lectins. Surfactant protein A (SP-A) is a collagen-containing C-type lectin, expressed by mucosal epithelial cells and mediates its antiviral activities by binding to viral glycoproteins.

Objective: This study examined the mechanistic role of human SP-A in SARS-CoV-2 infectivity and lung injury *in vitro* and *in vivo*.

Results: Human SP-A can bind both SARS-CoV-2 S protein and hACE2 in a dose-dependent manner ($p<0.01$). Pre-incubation of SARS-CoV-2 (Delta) with human SP-A inhibited virus binding and entry and reduced viral load in human lung epithelial cells, evidenced by the dose-dependent decrease in viral RNA, nucleocapsid protein (NP), and titer ($p<0.01$). We observed significant weight loss, increased viral burden, and mortality rate, and more severe lung injury in SARS-CoV-2 infected hACE2/SP-A KO mice (SP-A deficient mice with hACE2 transgene) compared to infected hACE2/mSP-A (K18) and hACE2/hSP-A1 ($6A^2$) mice (with both hACE2 and human SP-A1 transgenes) 6 Days Post-infection (DPI). Furthermore, increased SP-A level was observed in the saliva of COVID-19 patients compared to healthy controls ($p<0.05$), but severe COVID-19 patients had relatively lower SP-A levels than moderate COVID-19 patients ($p<0.05$).

Discussion: Collectively, human SP-A attenuates SARS-CoV-2-induced acute lung injury (ALI) by directly binding to the S protein and hACE2, and inhibiting its infectivity; and SP-A level in the saliva of COVID-19 patients might serve as a biomarker for COVID-19 severity.

KEYWORDS

acute lung injury, biomarker, COVID-19, innate immunity, SARS-CoV-2, spike protein, surfactant protein A

Introduction

More than 7 million people have died due to coronavirus disease 2019 (COVID-19), with the United States reporting more deaths than any other country. COVID-19 is an infectious disease caused by severe acute respiratory syndrome coronavirus 2 (SARS-CoV-2) (1). Previous studies have shown that morbidity and mortality following SARS-CoV-2 infection are predominantly due to a robust influx of inflammatory cells and cytokines into the lungs resulting in acute lung injury (ALI) and acute respiratory distress syndrome (ARDS) (2). SARS-CoV-2, like other coronaviruses, is an enveloped virus with several structural and non-structural proteins that facilitate its infectivity and pathogenicity in humans (3). Most important among the structural proteins for viral infectivity is the spike protein (S protein) which associates as a trimer on the viral envelope and is the basic unit through which the virus attaches to the host cellular receptor, human angiotensin-converting enzyme receptor 2 (hACE2), predominantly expressed on epithelial cells, including alveolar type II cells (ATII) in the lungs and in several other tissues (4). Each monomer of the S protein is composed of the S1 and S2 subunits. The S1 subunit contains the receptor-binding domain (RBD) which primarily binds to hACE2 while the S2 domain mediates the fusion of the viral and host cell membrane upon cleavage of the S protein subunit by the host transmembrane protease serine 2 (TMPRSS2) (5). Interestingly, as observed in most viral glycoproteins, the SARS-CoV-2 S protein is decorated with several N- and O-linked carbohydrate structures that have been demonstrated to protect it from antibody recognition (5, 6). While the presence of sugars on viral S protein can enable immune evasion, it may also enhance recognition by host innate immune carbohydrate-binding proteins (lectins), such as the human surfactant protein A (SP-A).

Human SP-A is a hydrophilic protein and belongs to the C-type lectin family of proteins (collectins) that surveys mucosal epithelial surfaces of the lungs, regions of the upper airway including laryngeal tissues, salivary glands, oral gingiva, and nasal mucosa, and bind to pathogen-associated molecular patterns (PAMPs) of most invading microbes (4, 7). Collectins such as surfactant proteins A and D (SP-A and SP-D) and mannose-binding lectin (MBL) are host humoral innate immune proteins that function by acting as a first line of defense against invading pathogens by binding to microbes and regulating inflammatory responses to maintain lung and other organs' health. Like other collectins, SP-A is composed of four functional domains among which is a carbohydrate recognition domain (CRD) that mediates Ca^{2+}-dependent binding to sugars on microbial glycoproteins (7). As a pattern recognition molecule (PRM), SP-A, alongside a related human lung-associated collectin (SP-D), has been demonstrated to bind sugar moieties on viral surfaces and inhibit their infectivity (7). Furthermore, SP-A enhances viral aggregation, opsonization, and lysis while modulating inflammation by interacting with various types of receptors on innate immune cells (7, 8). Several studies have described the antiviral and immunomodulatory activities of SP-A, SP-D, and MBL in the context of SARS-CoV-2, respiratory syncytial virus (RSV), Influenza A virus (IAV), human coronavirus 229E (HCoV-229E), and HIV (9–16). Interestingly, a recent *in silico* analysis showed that SP-A could ligate the S protein with an affinity similar to the ACE2-spike interaction (17), suggesting that SP-A may have an implication in the pathogenesis of SARS-CoV-2 infection. Previous studies demonstrated that SP-A can ameliorate RSV and IAV pathogenesis by enhancing viral clearance and modulating excessive inflammation, respectively (18, 19). Human SP-A has two functional genes (SP-A1 and SP-A2) with several genetic variants that have been observed at > 1% frequency in the general population: SP-A1 (variants 6A, $6A^2$, $6A^4$), and SP-A2 (variants $1A^0$, $1A^1$, $1A^3$) (20).

Given that the effectiveness of the newly developed vaccines and therapeutics for COVID-19 is continuously being threatened by the frequent emergence of SARS-CoV-2 variants with unique changes in the spike epitope that facilitate immune escape, there is a considerable ongoing global effort to develop and improve antivirals and immunomodulatory agents (21–23).

In this study, we hypothesized that SP-A plays a critical role in mucosal innate immunity against SARS-CoV-2 infectivity and acute lung injury. We found that human SP-A can bind both SARS-CoV-2 S protein and hACE2 and inhibit viral entry in susceptible human lung epithelial cells *in vitro*; and human SP-A can attenuate lung injury and viral burden using a double humanized transgenic mouse model (expressing hACE2 and human SP-A) following SARS-CoV-2 (Delta) infection. Moreover, increased SP-A level was observed in the saliva of COVID-19 patients. These findings contribute to our understanding of the role of human SP-A in SARS-CoV-2-induced pathogenesis as an important host defense protein that could attenuate SARS-CoV-2 infectivity and lung pathology while serving as a potential therapeutic component for COVID-19.

Results

SARS-CoV-2 S protein and RBD are recognized by human SP-A

SP-A activates host innate immunity by binding to pathogen-associated molecular patterns (PAMPs) such as glycan units on viral surface proteins. Given the profound level of glycosylation on SARS-CoV-2 S-protein (5), and SP-A binding to other respiratory viruses (10, 24); we examined the potential interaction of human SP-A with SARS-CoV-2 S protein and the RBD. As shown in Figure 1A, SP-A bound to SARS-CoV-2 S protein in a dose-dependent manner (0 -10 µg/ml of SP-A) in the presence of calcium (5 mM) but the binding of SP-A to S protein was reduced by 46% in the presence of 10 mM EDTA (a calcium ion chelator), suggesting that SP-A binding to S protein is slightly dependent on calcium (CRD domain) but other non-calcium-dependent regions might also play a role in S protein interaction because EDTA could not completely abrogate SP-A binding to S protein. Similarly, a dose-dependent binding of SP-A (0 - 10 µg/ml of SP-A) to immobilized SARS-CoV-2 RBD was also observed (Figure 1B). As shown in Figure 1B, 59% decrease in SP-A binding to the RBD was observed in the presence of 10 mM EDTA, suggesting the involvement of SP-A CRD and other domains in the interaction between SP-A and RBD.

10.3389/fimmu.2024.1370511

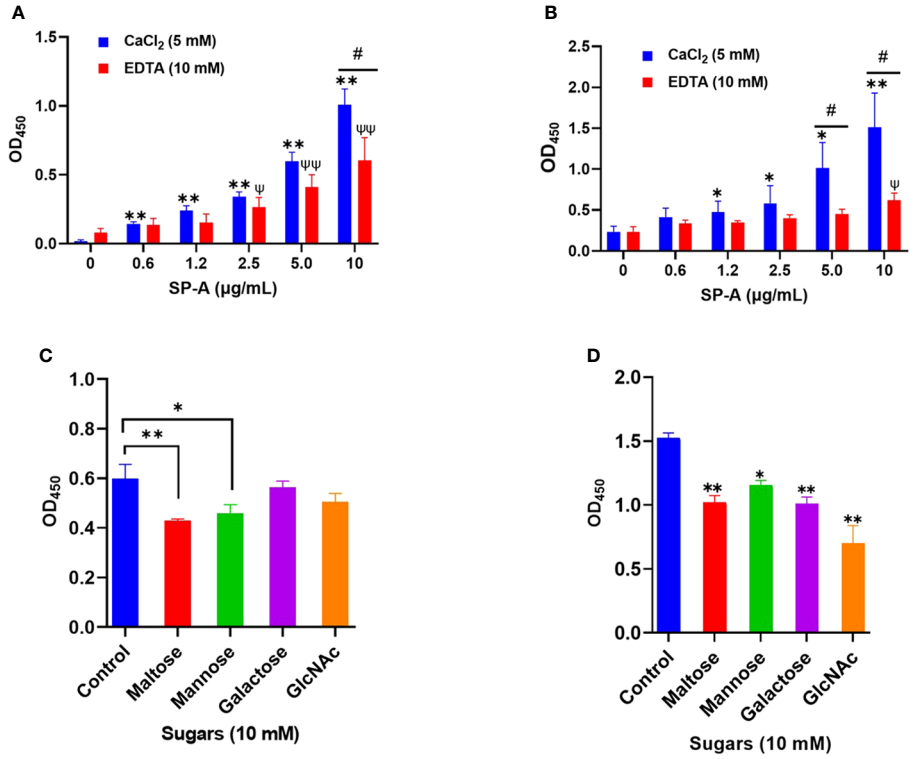

FIGURE 1
Human SP-A interacts with SARS-CoV-2 S protein and RBD. Purified S protein and RBD was immobilized on ELISA plates followed by incubation with serial dilutions of SP-A (0-10 µg/ml) in either 5 mM $CaCl_2$ or 10 mM EDTA-containing buffer. The data show a dose-dependent increase in SP-A binding to SARS-CoV-2 S protein **(A)** and RBD **(B)**. SARS-CoV-2 S protein **(C)** and RBD **(D)** coated plates were incubated with 10 µg/ml SP-A in the presence of 10 mM of each kind of sugar i.e. maltose, mannose, galactose, and N-acetylglucosamine (GlcNAc). Control samples were incubated, with SP-A in 5 mM $CaCl_2$ buffer without sugars and absorbance readings compared to control samples. Experiments were carried out in duplicates with three independent experiments. The data are presented as mean ± SE of 3 independent experiments. (*P<0.05; **P<0.01 reflect the levels of statistical significance in comparison with no SP-A treated group (0 µg/ml) in 5 mM $CaCl_2$-containing buffer by unpaired student's t-test analysis. ψ<0.05, ψψ<0.01 are the levels of significance compared to 0 µg/ml SP-A in 10 mM EDTA buffer while #<0.05 is the level of significance for the same SP-A concentrations in 5 mM $CaCl_2$ vs 10 mM EDTA-containing groups.

The binding of SP-A to SARS-CoV-2 S protein and RBD is inhibited by sugars

Each monomer of SARS-CoV-2 S protein has about 17 of its 22 N- glycosylation sites occupied by glycans with two O-linked glycan sites on the RBD (6). SP-A has various binding affinities for carbohydrate molecules. Thus, we hypothesized that SP-A binds to S protein and RBD by recognizing the sugars displayed on its surface. To demonstrate whether sugars can competitively inhibit SP-A recognition of S protein and RBD, we incubated SP-A with immobilized S protein and RBD in the presence of 10 mM sugars (maltose, mannose, galactose, and GlcNAc). In Figure 1C, a reduced SP-A binding to S protein was observed in the presence of maltose and mannose with no significant inhibition by Galactose and GlcNAc. However, SP-A recognition of RBD was inhibited by all the sugars tested (Figure 1D). Although, increasing concentrations of maltose could not completely abrogate SP-A interaction with S protein and RBD (Supplementary Figure E1 A, B). These data indicate that SP-A binds glycoconjugates on the S protein and RBD of SARS-CoV-2. However, there is also the potential for other forms of protein-protein interaction because of the observed interaction regardless of the presence or dose of sugars.

SP-A binds to hACE2 and impacts SARS-CoV-2 RBD interaction with hACE2 receptor

Since SARS-CoV-2 mainly infects hACE2-expressing airway and lung epithelial cells which are also the predominant SP-A-expressing cells; we assessed whether SP-A could interact with hACE2 directly. We observed a dose-dependent increase in SP-A binding to biotinylated hACE2 (Figure 2A). Furthermore, SP-A binding to hACE2 decreased significantly in the presence of EDTA, indicative of its reliance on calcium for optimum interaction with hACE2. However, Mannose, a preferred ligand for SP-A, showed a weak inhibitory effect on SP-A interaction with hACE2, suggesting that SP-A interaction with hACE2 may act through glycoconjugate and non-glycoconjugate binding (Supplementary Figure E2). Given that SP-A can bind hACE2, we further examined its impact on the interaction between SARS-CoV-2 RBD and hACE2 by simultaneously incubating SP-A and hACE2 on ELISA plates immobilized with RBD. We observed a reduced hACE2 binding to RBD in the presence of SP-A while BSA (used as a control for non-specific protein interaction) had no inhibitory effect on RBD-hACE2 interaction (Figure 2B). Therefore, SP-A can interfere with the interaction between RBD and hACE2.

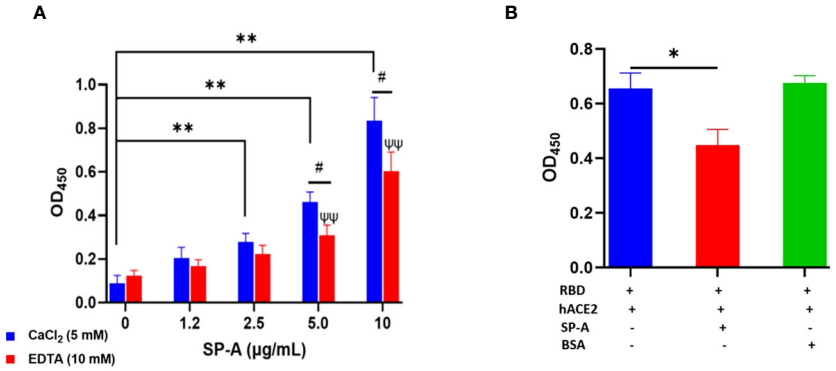

FIGURE 2
SP-A binds to hACE2 and impacts the interaction of SARS-CoV-2 RBD and hACE2. **(A)** Microtiter plates were coated with biotinylated hACE2 (0.2 μg/ml) and plates were then incubated with a range of SP-A concentrations (0-10 μg/ml) in the presence of 5 mM calcium or 10 mM EDTA, and the level of bound SP-A was detected as described previously. **(B)** SP-A (10 μg/ml) was simultaneously incubated with biotinylated hACE2 (10 μg/ml) in wells immobilized with RBD (5 μg/ml). To assess non-specific protein interaction, some wells were incubated with 10 μg/ml BSA. Statistical analysis was performed by a student's t-test. Values are mean ± SEM (*P<0.05, **P<0.01 compared to 0 μg/ml SP-A in $CaCl_2$-containing group. ψψ<0.01 vs 0 μg/ml SP-A in 10 mM EDTA group while #<0.05 is the level of significance for same SP-A concentrations in 5 mM $CaCl_2$ vs 10 mM EDTA-containing groups.

Human SP-A inhibits binding and entry of SARS-CoV-2 pseudotyped particles and SARS-CoV-2 (delta variant) in host cells

The ELISA showed that SP-A binds to SARS-CoV-2 S protein and RBD, as well as interfere with RBD-hACE2 interaction. We further examined whether SP-A could inhibit SARS-CoV-2 infectivity using both pseudotyped particles and infectious SARS-CoV-2 (Delta variant). It is known that glycans adjacent to the RBD can serve as determinants of viral binding with cellular receptors to facilitate subsequent entry (25), and SP-A interaction with RBD was attenuated in the presence of sugars which suggests that SARS-CoV-2 entry in hACE2-expressing host cells may be inhibited by pre-treating with SP-A. Thus, we assessed whether the capacity of SP-A to bind S protein and RBD can result in viral entry inhibition. We challenged HEK293T-ACE2+TMPRSS2 and A549-ACE2 cell lines with a luciferase- or GFP-tagged SARS-CoV-2 pseudotyped particle (expressing wildtype (WT) S protein on its surface) pre-incubated with or without SP-A and observed significantly reduced luciferase intensity in an SP-A dose-dependent manner starting at 6.25 μg/ml in HEK293-ACE2+ TMPRSS2 (Figure 3A) and 12.5 μg/ml in A549-ACE2 (Figure 3B). As shown in Figures 3C, D, we also observed a decrease in GFP intensity with increasing SP-A concentrations in a dose-dependent manner in HEK-293T-ACE2 cells.

To further validate the role of SP-A in SARS-CoV-2 infectivity, binding, and entry assays with an infectious SARS-CoV-2 (B.1.617.2, Delta variant) were performed. We observed that the level of viral particles bound on the cell surface decreased significantly in a dose-dependent manner compared to the BSA-treated and untreated (0 μg/ml) controls at 4°C (Figure 4A). Temperature shift experiments at 37°C for 1 h showed lower levels of internalized viral RNA with increasing SP-A concentrations (Figure 4B). This level of the internalized virus was reduced by ≈ 58% relative to control (0 μg/ml) in cells inoculated with virus + 25 μg/ml SP-A. Before shifting to 37°C, we validated viral entry by treating some cells inoculated with virus only (0 μg/ml SP-A) with proteinase K to remove virus on the cell surface after the 4°C incubation (binding control) and observed only minimal levels of bound viruses. As previously described with pseudotyped viruses, pre-incubation of virus with increasing SP-A concentrations (0 to 50 μg/ml) before inoculating confluent A549-ACE2 cells resulted in a dose-dependent decrease in SARS-CoV-2 N protein (NP) levels in cells 4 hpi (Figures 4C, D). As expected, Chloroquine (CQ), an established inhibitor of SARS-CoV-2 entry used as a positive control, inhibited virus entry. The results highlight the binding and entry inhibitory activity of SP-A in the context of SARS-CoV-2 infection.

Human SP-A attenuates SARS-CoV-2 infectivity in A549-ACE2 cells

The hallmark of viral infectivity is the ability to not merely get into a cell but to also replicate its genome, express both structural and non-structural proteins, and assemble these components to produce infectious progeny viral particles. We therefore investigated the potential inhibitory role of SP-A in SARS-CoV-2 infectivity by RT-qPCR, immunoblotting and plaque assay using total RNA and protein isolated from infected cells and supernatant 24 h after infection of A549-ACE2 cells. The results showed that SP-A significantly reduced SARS-CoV-2 RNA level in cells in a dose-dependent manner (0 – 50 μg/ml of SP-A) (Figure 5A). In the presence of 50 μg/ml SP-A, we observed approximately 50% decrease in viral RNA level in cells. These results were further confirmed by immunoblotting assay where a dose-dependent decrease in the level of SARS-CoV-2 NP was observed (Figures 5B, C). 50 μg/ml SP-A resulted in an approximately 10-fold reduction in virus titer compared to cells infected with the virus only by plaque assay (Figures 5D, E). Taken together, these results

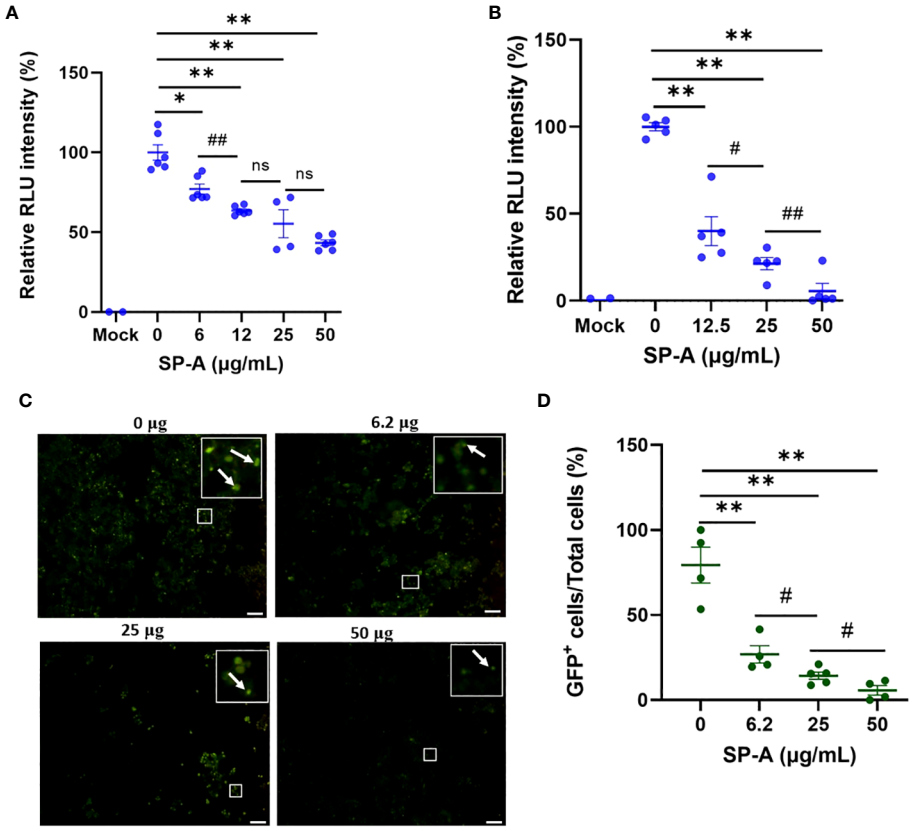

FIGURE 3
SP-A inhibits entry of SARS-CoV-2 pseudotyped lentiviral particles in susceptible host cells. We measured the luciferase intensity of the SP-A (0-50 µg/ml) pre-treated WT S protein pseudotyped lentiviral particles in the cell lines: **(A)** HEK293T-ACE2+TMPRSS2; **(B)** A549-ACE2. **(C)** Representative images of GFP-positive cells in HEK293T-ACE2+TMPRSS2 challenged with SP-A pre-treated and un-treated GFP-tagged SARS-CoV-2 pseudotyped particles. **(D)** GFP signal taken from 10 images per well, normalized to the cellular area and quantified by Image J software. The data were expressed as mean ± SEM of the percentage of positive cells/total cells per area analyzed (n=3). Scale bar = 100 µm. *P<0.05; **P<0.01, compared to control sample (0 µg/ml). #<0.05, ##<0.01, compared between two SP-A doses. ns = not significant.

suggest that human SP-A has an inhibitory effect on SARS-CoV-2 entry and reduces viral load in human lung epithelial cells by interacting with SARS-CoV-2 S protein and preventing viral binding to A549-ACE2 cells.

SP-A deficient mice are more susceptible to SARS-CoV-2-induced acute lung injury

Three types of hACE2 transgenic mice with either no SP-A (hACE2/SP-A KO), mouse SP-A (hACE2/mSP-A, K18), or human SP-A (hACE2/SP-A1 ($6A^2$) background were intranasally infected with 1×10^3 PFU of SARS-CoV-2 (Delta variant) and monitored for body weight changes, and survival for 10 days. We observed remarkable weight loss starting on day 4 post-infection, with a drastic decline on days 5 and 6 post-infection especially in hACE2/SP-A KO mice. Weight loss peaked on 6 DPI for all SARS-CoV-2 infected groups, particularly in hACE2/SP-A KO mice (15.1 ± 7.3%), hACE2/mSP-A (5.2 ± 8.3%), and hACE2/hSP-A-1 ($6A^2$) (6.86 ± 6.9%) (Figure 6A). This tendency in weight loss continued until day 9 and increased on day 10. However, none of the KO mice regained their weights or survived beyond 9 dpi in this study. Besides weight loss, other clinical signs observed were ruffled fur, hunched posture, difficulty breathing, lethargy, ocular discharge, tremor, and severe intestinal bloating in the most severe cases starting at 3 DPI. These symptoms were particularly severe in SP-A KO mice compared to those mice with hSP-A or mSP-A gene. Most of the SP-A KO mice succumbed to the infection on 6 DPI or reached IACUC-defined endpoints for survival and were euthanized. Notably, barely 50% of SP-A deficient mice survived on day 6 compared to 100% survival observed in mice carrying human SP-A (Figure 6B). To assess SARS-CoV-2 induced ALI, lung sections of mice from each group (n=6-7/group) were examined as previously described (26). Lung histopathological analysis showed normal lung histology in all Sham groups. SARS-CoV-2 infection 6 DPI resulted in severe lung injury, characterized by a diffused influx of inflammatory cells in airspaces and interstitial, pulmonary hemorrhage, alveolar septal thickening, and an accumulation of proteinaceous debris and edema within the alveoli and interstitial. SARS-CoV-2-induced ALI was particularly severe in hACE2 Tg mice deficient in SP-A compared to mice with mSP-A or hSP-A (Figure 6C). An evaluation of infected mice showed that hACE2/mSP-A (K18) and hACE2/hSP-A 1 ($6A^2$) mice had similar lung injury scores while hACE2/SP-A KO had a more significantly

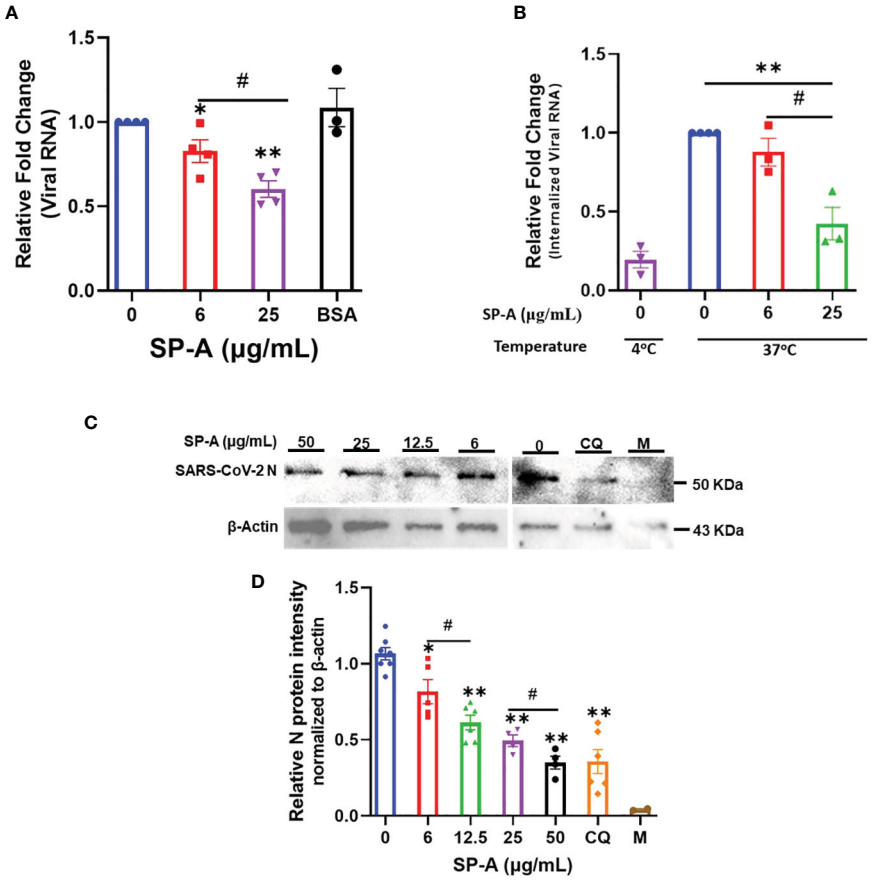

FIGURE 4
SP-A attenuates SARS-CoV-2 (Delta) binding and entry in A549-ACE2 cells. **(A)** Viral binding assays were performed in A549-ACE2 cells. SARS-CoV-2 (Delta variant) was pre-incubated with the indicated concentrations of SP-A or BSA (used as a non-specific protein control, 50 µg/ml) for 1h at RT. Then inoculated onto pre-chilled cells for another 2 h at 4°C to allow binding to the cell surface. **(B)** Viral entry assays were performed as described above. However, after 2 h incubation of SP-A + virus mixture at 4°C, the cells were washed, and fresh media was added and shifted to 37°C for 1 h to allow virus entry into cells. The cells were washed and treated with proteinase K (1 mg/ml) to remove attached viral particles on the cell surface and the amount of internalized viral particles was quantified by RT-qPCR. Binding control at 4°C was also used to assess virus entry by treating cells inoculated with virus only (0 µg/ml SP-A) after 2 h incubation with proteinase K prior to shifting to 37°C. The relative fold change was normalized to 18S rRNA internal control and expressed as mean ± SEM of the relative fold change in CT values compared to the control sample (0 µg/ml). **(C)** A549-ACE2 cells inoculated with SP-A + virus mixture for 2h and then cells were harvested after 4 h incubation for Western blotting analysis using SARS-CoV-2 N protein and β-actin antibodies, respectively. Representative images of Western blotting analysis of cell lysates with SARS-CoV-2 N protein and β-actin as a control. Chloroquine (CQ) (10 µM) was used as a positive control. **(D)** Quantification of N protein level relative to β-actin (loading control). Each data represents the relative mean ± S.E. *P<0.05; **P<0.01, compared to control group (0 µg/ml); #<0.05= significance between two doses.

higher lung injury score than hACE2/mSP-A (K18) and hACE2/hSP-A 1 ($6A^2$) mice (P<0.01) (Figure 6D). We also assessed the amount and distribution of SARS-CoV-2 NP in infected lung lesions by immunohistochemistry (IHC). While no SARS-CoV-2 NP was observed in control (Sham) mice, there was widespread viral dissemination in the lungs of SP-A deficient hACE2 Tg. The lesions positive for SARS-CoV-2 NP were more diffuse in mice without SP-A than in K18 and humanized SP-A mouse lines. In general, we observed a very low, localized presence of SARS-CoV2-2 NP in hACE2/hSP-A mice compared to hACE2/SP-A KO and hACE2/mSP-A mice (Figures 6F, G).

To compare body weight loss and ALI score with SARS-CoV-2 titers, we infected each mouse group with SARS-CoV-2 (Delta variant) (n=6-7/group) and sacrificed at 6 DPI. Lungs were dissected and homogenized, and supernatants from lung homogenates were subjected to RT-qPCR and plaque assay. Viral RNA load was comparable in hACE2 Tg mice with mSP-A (K18) and hSP-A backgrounds compared with the significantly elevated SARS-CoV-2 RNA loads in SP-A deficient hACE2 Tg mice (Figure 6E). Infectious virus titer in hACE2/SP-A KO and hACE2/mSP-A (K18) was ~ 1×10^3 PFU in lung tissues while mainly undetectable in most hACE2/hSP-A1 ($6A^2$) mice (Supplementary Figure E3).

We also observed significantly higher TNF-α and IL-6 in the infected KO mice compared to the infected K18 and hSP-A mice (Figures 6H, I); indeed, there was no change in the level of IL-6 in infected $6A^2$ relative to Sham, supporting the role of elevated IL-6 as a major contributor to severe disease observed in COVID-19 patients (27, 28). The results highlight the crucial role of human SP-A in attenuating the severity of SARS-CoV-2-induced ALI by decreasing viral burden and modulating inflammatory responses in the lungs of infected mice.

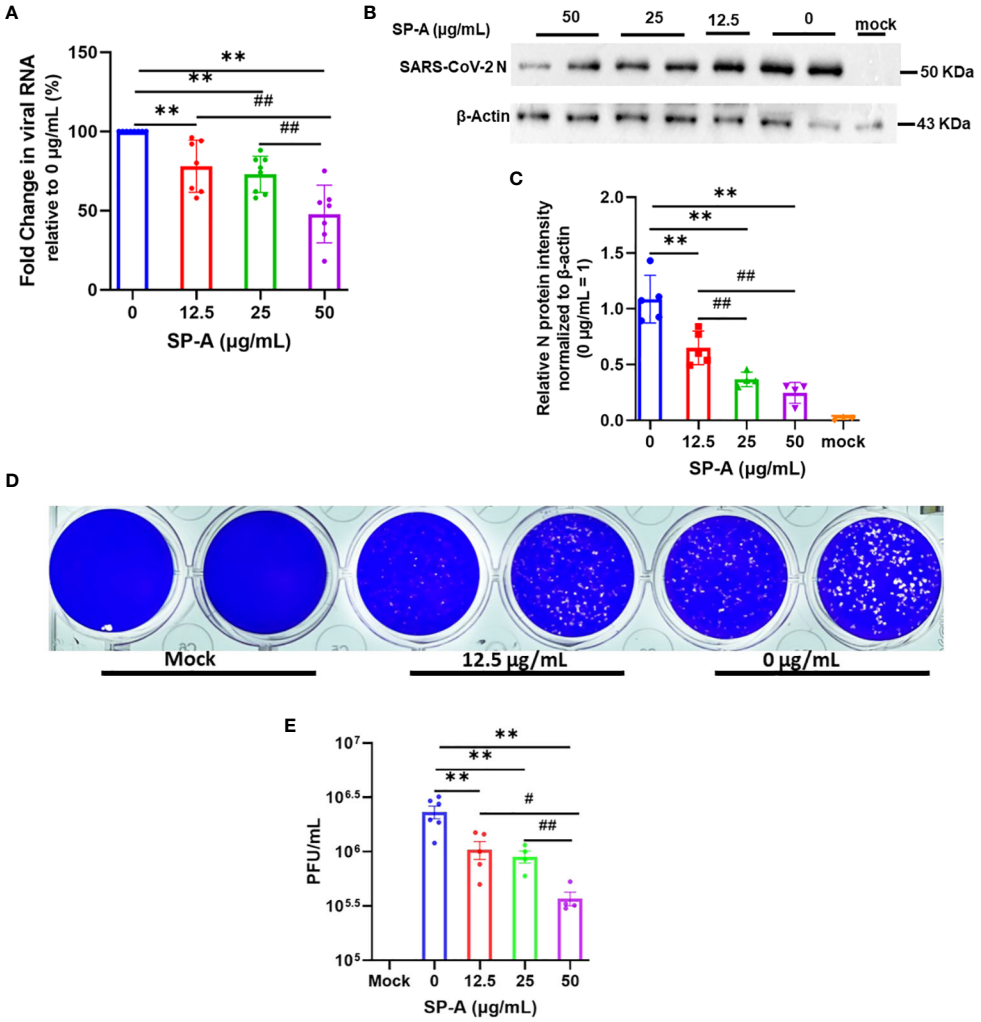

FIGURE 5
SP-A inhibits SARS-CoV-2 (Delta) infectivity in A549-ACE2. SARS-CoV-2 was pre-incubated with increasing concentrations of SP-A before inoculating A549-ACE2. Cell culture media and cells were collected and used for RT-qPCR, western blot, and plaque assays. **(A)**: Significant decrease in viral RNA levels in A549-ACE2 cells treated with or without SP-A and expressed as fold change in CT values relative to control (0 µg/ml) 24h hpi. **(B)**: Western blots of SARS-CoV-2 N expressions in cell lysates treated with increasing concentrations of SP-A **(C)**: Relative viral N protein levels in A549-ACE2 cell lysate normalized to β-actin. **(D)**: Visible plaques on Vero E6 cells infected with or without (0 µg/ml) SP-A. **(E)**: Dose-dependent decrease in virus titer with increasing SP-A concentrations. Values represent mean ± S.E. **P<0.01, compared to the control sample (0 µg/ml) and #<0.05, ##<0.01 when compared between two concentrations (n= 3).

Increased SP-A level in the saliva of COVID-19 patients compared to healthy controls

Changes in pulmonary surfactant protein levels and elevated MBL in the sera of some SARS and COVID-19 patients have been shown to correlate with disease severity (29–33). Thus, we examined the level of SP-A in the saliva of COVID-19 patients hospitalized with varying disease severity. The results showed that COVID-19 patients have an elevated total protein levels in their saliva compared to healthy controls (Figure 7A), which was particularly higher in severe patients upon stratification based on disease severity (Figure 7B). SP-A levels in COVID-19 patients were higher relative to healthy controls (Figure 7C). However, we observed a profoundly reduced SP-A level in the subgroup of severe COVID-19 patients (Figure 7D), despite the higher total protein levels observed in this subgroup; highlighting the importance of a relatively preserved level of SP-A in the salivary mucosa of SARS-CoV-2 infected individuals to alleviate the most severe COVID-19 symptomology.

Discussion

Barely four years since first reported, COVID-19 has become one of the leading causes of death in the US (1). The goal of current antiviral research is to develop novel therapies that not only target viral proteins but also important host proteins/pathways that are essential for the virus's life cycle (23, 34). As the current COVID-19 pandemic has highlighted with the frequent emergence of variants

10.3389/fimmu.2024.1370511

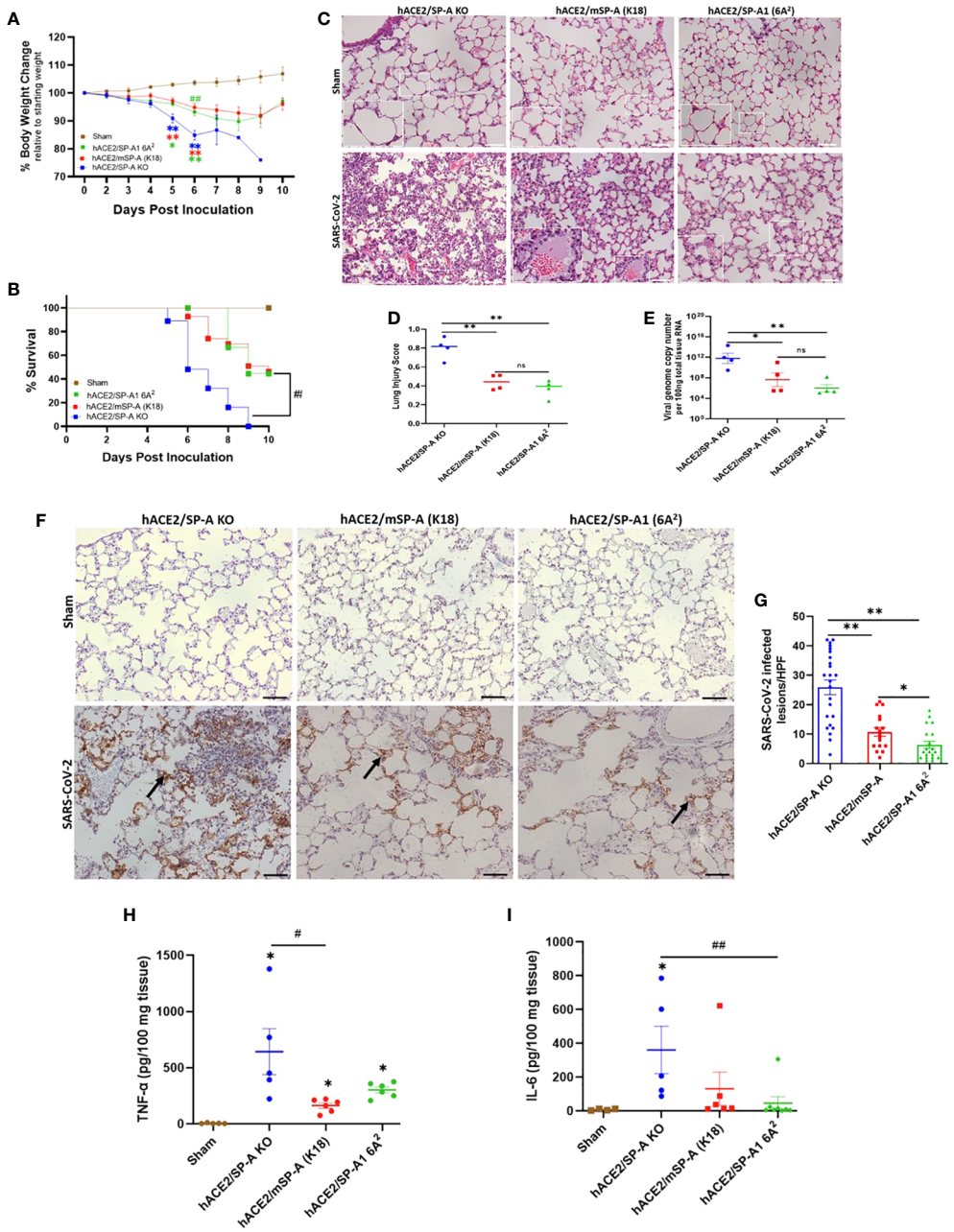

FIGURE 6
SP-A attenuates the severity of SARS-CoV-2-induced acute lung injury *in vivo*. Three groups of mice (hACE2/SP-A KO, hACE2/mSP-A, and hACE2/hSP-A 1 ($6A^2$) were infected intranasally with 1×10^3 PFU of SARS-CoV-2 (Delta) and sacrificed on day 6 P.I or monitored until day 10 for survival study. **(A)** Significant weight loss was observed in all infected mice relative to sham controls starting on day 5. However, on day 6, a more dramatic weight loss was observed in KO relative to hSP-A mice. Body weight change was monitored daily and compared with the initial weight on day 0. **(B)** Significant mortality was observed in SP-A KO mice compared to K18 and hSP-A mice. **(C)** Representative histological images of lung sections from each group indicating normal lung structures in all Sham groups. SARS-CoV-2-induced lung damage was marked by an infiltration of inflammatory cells into the alveoli and interstitial, pulmonary hemorrhage, accumulation of proteinaceous debris, and interstitial edema in infected mice (n=6-7 per group). **(D)** Semi-quantitative histological lung injury score was evaluated. There was no significant pathology in sham group. A significantly higher lung injury score was observed in SP-A deficient mice compared to hACE2 transgenic mice with either mSP-A or hSP-A. **(E)** Viral RNA levels quantified by RT-qPCR. **(F)** Representative IHC images of SARS-CoV-2 NP in infected mice with diffuse SARS-CoV-2 antigen within alveolar airspaces and interstitial, particularly in hACE2 Tg SP-A KO mice (arrows) and NP positive lesions were quantified **(G)**. Bar graphs of absolute concentrations of TNF-α **(H)** and IL-6 **(I)** using ELISA in the lungs of infected and sham mice 6 DPI. Scale bars = 50μm. N = 15-20 mice/group for body weight and survival studies. Symbols represent data from each individual mouse and bars represents means ± S.E. from 3 independent experiments. *P<0.05, **P<0.01. #<0.05, ##<0.01, compared between two infected mouse groups. ns = not significant.

10.3389/fimmu.2024.1370511

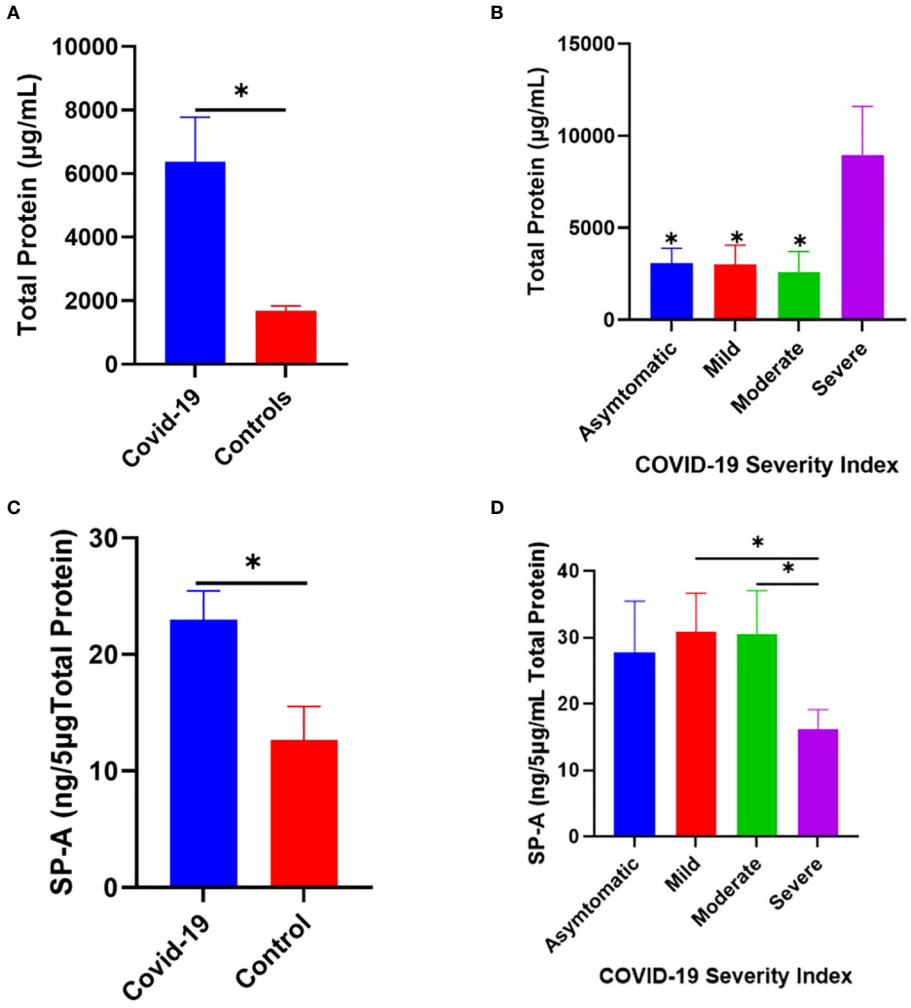

FIGURE 7
Increased SP-A level in the saliva of COVID-19 patients compared to healthy control. **(A)** Higher total protein concentration in the saliva of COVID-19 patients (n=40) and healthy controls (n=12). **(B)** Severe COVID-19 patients have significantly elevated total protein compared to asymptomatic, mild, and moderately infected patients. **(C)** Higher SP-A levels in the saliva of COVID-19 patients compared with healthy controls. **(D)** Upon stratification, severe patients had significantly reduced SP-A levels compared to mild and moderate patients. *p<0.05, compared between COVID-19 and healthy controls or between two COVID-19 groups.

with potential for immune escape, there is the need to rather focus on host antiviral proteins (23, 34). Moreover, the potential of using lectins (carbohydrate-binding proteins) has gained huge appeal in recent times since these molecules interact with relatively conserved glycoconjugates on viral proteins to mediate their antimicrobial functions (35). Thus, lectins are less sensitive to loss of function mutations due to sequence changes in viral surface proteins required for cellular entry and replication. Interestingly SP-D, a related collectin, was recently shown to inhibit SARS-CoV-2 entry and replication in host cells (13, 14). Therefore, we hypothesized that SP-A can bind to SARS-CoV-2 S protein and this interaction will attenuate SARS-CoV-2 infectivity and lung pathology in susceptible host cells and animals.

For the first time, our findings demonstrate that human SP-A can bind SARS-CoV-2 S protein and RBD in a dose-dependent manner. The biological significance of SP-A binding to SARS-CoV-2 S protein was emphasized by its inhibitory effect on viral infectivity in a lung epithelial cell line. Compared to RBD, we observed that SP-A interaction with the S protein is less dependent on calcium ions. The significantly reduced SP-A binding to RBD observed in the presence of the calcium ion chelator, EDTA, and binding competitors (sugars), signifies the involvement of the CRD whose binding capacity to glycans is dependent on divalent ions like calcium. Notably, the SARS-CoV-2 RBD is a 223 peptide (amino acid sequence from 319 to 541 of S protein), which might have influenced the capacity of other regions of the bouquet-shaped SP-A to recognize it (5). Meanwhile, the calcium-independent binding to the S protein observed in our study is in line with previous reports of SP-A's interactions with the glycoproteins of IAV and HIV (though at low pH) (11, 12). Benne and colleagues previously showed that SP-A interacts with sialic acids in the hemagglutinin of IAV through its collagen-like domain (11). Our finding is novel because SP-A only partially recognized the S protein of a closely related beta coronavirus, SARS-CoV-1; while SP-D bound strongly with SARS-CoV-1 S protein (36).

Since hACE2-expressing cells are the major targets for SARS-CoV-2 infection, we tested whether SP-A can interact with hACE2 and the role of SP-A in RBD-hACE2 interaction. We observed a calcium-dependent binding of SP-A to hACE2. This could indicate that SP-A also binds to hACE2 through a CRD-dependent mechanism. Importantly, the observation that SP-A can competitively attenuate RBD-hACE2 interaction supports the idea that SP-A may interfere with SARS-CoV-2 interaction with the host hACE2 receptors.

We next assessed the biological significance of SP-A binding with SARS-CoV-2 S protein by pre-incubating pseudotyped and infectious SARS-CoV-2 (Delta) with SP-A before cellular challenge. The delta variant was used for this experiment and in our infectivity assays because of the profound pathogenesis induced by this variant both in the human population and in *in vitro* and *in vivo* models of infection (37–39). In examining the early events that occur upon SP-A interaction with SARS-CoV-2, we have uncovered that SP-A binding to SARS-CoV-2 RBD can impair viral binding and entry in lung epithelial cells, ultimately resulting in low viral load in cells. Besides the low levels of viruses bound to cells surface at 4°C in the presence of SP-A, we observed significantly reduced viral RNA in cells 1 h after infection at 37°C compared to SP-A untreated controls. At 1 hpi, whatever viral gene detected in cells is reasoned to have been introduced by the infecting particles and not a result of viral replication in the infected cells which was supported by the reduced viral N protein 4 hpi in A549-ACE2 cells challenged with SP-A pre-treated virus (40). These findings strongly suggest that the interaction between SP-A and viral S protein may have obstructed viral attachment to hACE2 on susceptible host cells, inhibiting SARS-CoV-2 entry as was previously observed with SP-A binding to HIV gp120 to prevent its interaction with $CD4^+$ cells (12).

However, beyond binding and entry, a viral infection is deemed successful following genome replication, expression of structural and non-structural proteins, packaging of viral components, and release of infectious progeny viral particles. Our RT-qPCR, immunoblot, and plaque assays all demonstrate the inhibitory effect of SP-A on SARS-CoV-2 infectivity by the observed low levels of RNA, NP, and virus titer upon SP-A pre-treatment. The approximately 10-fold decrease in infectious virus titers and approximately 50% reduction in viral RNA at 50 μg/ml SP-A is quite outstanding and we speculate that the reduction in SARS-CoV-2 binding, and entry by SP-A resulted in the significantly low levels of virus load in permissive lung epithelial cells as was previously observed with HCoV-229E, IAV, and RSV upon treating with collectins (9–11, 41).

This study focused on pre-treating SARS-CoV-2 with SP-A before cellular challenge and the downstream effects on infectivity. However, a previous report showed that some lectins are more potent inhibitors of virus infection when cells are treated with lectins as against virus treatment before infection (42, 43). Since our ELISA assays showed that SP-A can recognize hACE2 receptors and interfere with RBD-hACE2 interaction, further mechanistic studies to characterize the antiviral effect of SP-A by pre-treating cells before SARS-CoV-2 challenge and the complexity of such an interaction merits further studies.

Using three groups of mice, we evaluated the role of SP-A in SARS-CoV-2-induced lung damage. First, to remove the mSP-A gene, we first crossed hACE2/mSP-A Tg (K18) mice with our SP-A KO mice. Then we bred the characterized hACE2/SP-A KO mice with our lab's hTG SP-A1 ($6A^2$) mouse line to generate mice with both hACE2 and hSP-A1 ($6A^2$) transgenes (double-hTG). Using this double-hTG mouse line enabled us to have mice that are susceptible to SARS-CoV-2 infection while also allowing us to study the role of hSP-A. Our results show that the three mouse groups are highly susceptible to SARS-CoV-2 infection. However, compared to K18 and hACE2/$6A^2$ mice, mice deficient in SP-A quickly succumbed to infection by 6 DPI at 10^3 PFU as reflected by the sharp decline in body weight and mortality (> 40%). Histopathological analysis revealed moderate but comparable lung pathology in hACE2/$6A^2$ and hACE2/mSP-A (K18) mice, with severe lung pathology in hACE2 Tg mice deficient in SP-A. Interestingly, viral load analysis showed a correlation between high viral titers in the lungs and disease severity: hACE2/SP-A KO mice had significantly higher viral titers. However, we did not detect live virus at day 6 pi in our hACE2/$6A^2$ mice even with mean viral RNA levels reaching 10^6 copies. The absence of SP-A in the lungs of SP-A KO mice may have impacted the effective clearance of SARS-CoV-2 while leaving viral-induced inflammation unchecked as was previously observed with RSV (18), and demonstrated in our *in vitro* studies with lung epithelial cells. A previous study showed that viral titer peaked in the lungs of K18 mice on day 2 post infection and declines thereafter in K18 mice (44); supporting our finding of low infectious titers in our mouse groups 6 DPI.

Interestingly, the same cells i.e. ATII cells that mainly produce and secrete collectins are also the predominant lung epithelial cells targeted by SARS-CoV-2 (2, 45). Infection and subsequent damage of these cells results in decreased production and secretion of lung collectins, rendering the lung more susceptible to injury (32, 46–48). The importance of surfactant proteins has been demonstrated by the routine administration of surfactant-based replacement therapies in neonates with impaired lung functions (49). Thus, we assessed the levels of SP-A in the saliva of a subset of COVID-19 patients. Compared to controls, COVID-19 patients had relatively higher SP-A levels in their saliva, an increase that is suggestive of SP-A's innate immune roles during an acute infection prior to the induction of the adaptive immune response. However, patients with severe disease had remarkably reduced SP-A levels compared to moderately and mildly infected patients. We thus speculate that basal levels of SP-A in salivary mucosal are increased upon SARS-CoV-2 infection; however, in severe patients, SP-A levels are remarkably depleted due to reduced expression or more degradation (50), thus impairing host innate antiviral response. A dysregulation in essential surfactant protein (SP) genes among COVID-19 patients has also been observed (51).

A limitation of our study is the small size of human saliva specimens used in this study, and that we do not know the time from infection to symptomology and hospitalization among our study participants and as a result cannot definitively link low SP-A levels to disease severity. For example, it could be reasoned that severe patients with low SP-A levels may have been hospitalized longer and may have had other pre-existing conditions and co-

infections that could have seriously impacted SP-A levels in their saliva. Reactive compounds generated during inflammatory processes have been shown to alter the structure and function of surfactant proteins. Thus, another limitation of this study is the low volume of saliva obtained from the COVID-19 patients which has impacted our ability to conduct further biochemical studies of SP-A oligomerization and the impact on disease severity. Indeed, SARS-CoV-2 infection results in profound lymphocytopenia, that can predispose individuals to secondary infections by otherwise relatively nonpathogenic and pathogenic bacteria (52). In addition, there have been several reports of bacterial coinfections among very severe COVID-19 patients in the ICU (53, 54). The higher tendency for secondary bacterial infections among COVID-19 patients might be due to epithelial cell damage and/or alterations in host innate immune molecules and should be further investigated.

Several studies have previously shown that levels of collectins among the general population vary depending on an individual's unique SP variant and this could result in differential SP-A levels (55). Structural and functional changes in surfactant proteins have been linked to single nucleotide polymorphisms demonstrated to affect their abilities to bind microbial PAMPs and carbohydrates (56). These polymorphisms in SP genes may influence their interactions with SARS-CoV-2 glycoproteins and future research should focus on elucidating the ability of SP-A variants to interact with SARS-CoV-2 glycoproteins and the functional roles of the variants on viral infectivity and pathogenesis both *in vitro* and *in vivo*. Moreover, since several SARS-CoV-2 variants have been observed with mutations in their S protein demonstrated to confer resistance to neutralization antibodies (21, 22, 57), it could mean that changes in S protein can remove or introduce novel N- and O-glycosylation sites that could potentially make the S protein more or less sensitive to collectins as observed previously with IAV strains and SARS-CoV-2 (6, 16, 58, 59). To address this possibility, further studies should examine mechanistically SP-A interactions with SARS-CoV-2 variants and the biological significance using both *in vitro* and animal models of infection.

In conclusion, these findings demonstrate the mucosal innate immunity of human SP-A in attenuating SARS-CoV-2-induced lung injury by interacting with S protein and inhibiting viral infectivity (Figure 8). These findings supplement current efforts aimed at developing novel surfactant-based therapies to combat COVID-19.

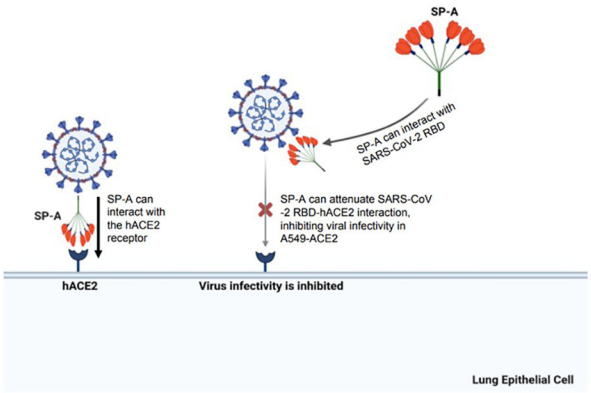

FIGURE 8
A diagram of SP-A interaction with S protein and human ACE2 receptor resulting in a significant decrease in SARS-CoV-2 infectivity. The SARS-CoV-2 spike protein can be recognized by human SP-A resulting in viral particle aggregations and reduced interactions of virus and host cell ACE2 receptors. Human SP-A also directly interacts with the human ACE2 receptor, reducing binding of SARS-CoV-2 RBD to hACE2, and subsequently diminishing viral entry and infectivity in susceptible host cells.

Materials and methods

Human SP-A protein

Native human SP-A (hSP-A) was isolated and purified from bronchoalveolar lavage fluid (BALF) of alveolar proteinosis patients as described previously (60). The purity of the SP-A preparation was confirmed by SDS-PAGE followed by silver staining and then filtered through a 0.2-micron filter to remove potential contaminants.

Cells and viruses

HEK293T-ACE2+TMPRSS2 (human embryonic kidney cell line overexpressing both human ACE2 and TMPRSS2 genes) and A549-ACE2 (human lung carcinoma epithelial cell overexpressing human ACE2, BEI Resources, NIAID) and Vero E6 cells (BEI resources, NIAID) were cultured and maintained in GlutaMax Dulbecco's modified Eagle's medium (DMEM) containing 1g/L D-glucose and 110mg/L sodium pyruvate supplemented with 10% (v/v) fetal bovine serum (FBS) and 1% (v/v) antibiotic (100U/mL of penicillin and 100µg/mL of streptomycin, Gibco) at 37°C and 5% CO_2 atmosphere. SARS-CoV-2 (B.1.617.2, 1.8×10^6 PFU/ml, P3) used in this study was obtained from the World Reference Center for Arboviruses (WRCEVA) and was propagated in Vero E6 cells under BSL-3 containment conditions. Plaque forming assay (PFU) was performed to determine viral titer.

Generation of hACE2 and TMPRSS2-stably expressing HEK-293T cells

HEK293/ACE2/TMPRSS2 cell line, which is stable-producing human ACE2 and co-receptor, TMPRSS2, is a kind gift from Dr. Marc C Johnson of University of Missouri (61).

Production of luciferase- and GFP-tagged pseudotyped particles

SARS-CoV-2 S protein gene expressing cDNA (gift from Dr. Marc Johnson, University of Missouri School of Medicine) was used to pseudotype Feline immunodeficiency virus (FIV) expressing

luciferase (ScV2 S-FIV-mCherry/Luc) or green fluorescent protein (ScV2 S-FIV-GFP) by using previously described methods (61, 62).

Animal models

The mice used in this study were bred and maintained in the animal core facility at SUNY Upstate Medical University. Mice were housed in temperature-controlled room at 22°C under specific pathogen-free conditions. 8–24 weeks old male and female mice were used in this study. The animal experiments were approved by the Institutional Animal Care and Use Committee of the SUNY Upstate Medical University with protocol #507 and were performed according to the National Institutes of Health and ARRIVE guidelines on the use of laboratory animals. The original hACE2/mSP-A (K18) mice were purchased from Jackson Laboratories (Bar Harbor, ME). K18 mice are highly susceptible to SARS-CoV-2 infection with similar pathological outcomes as seen in mild to moderate COVID-19 patients. However, K18 mice have mouse SP-A (mSP-A) background. To study the role of human SP-A (hSP-A), we generated mice with both hACE2 and hSP-A background (double humanized transgenic (double-hTG) mice expressing hACE2 and a single gene variant of hSP-A1 ($6A^2$) without mouse SP-A background by breeding with our previously generated hTG SP-A mice. Briefly, we first crossed K18 (hACE2/mSP-A) mice that are hemizygous for the hACE2 transgene with our human SP-A knockout (KO) mice to remove mSP-A gene. Genotyping was performed after each filial generation. Subsequently, we crossed the hACE2/SP-A KO mice with hSP-A1 ($6A^2$ variant) to generate double-hTG mice with hACE2 and hSP-A transgenes. We examined hACE2 and hSP-A1 ($6A^2$) genes in the mice by PCR genotyping analysis using DNAs isolated from mouse tail biopsy and analyzed lung SP-A expression by Western blotting. This double-hTG (hACE2/hSP-A1 ($6A^2$) variant alongside hACE2/SP-A KO and hACE2/mSP-A (K18) mice were used for subsequent challenge studies with SARS-CoV-2 delta variant.

Mouse infection and sample processing

SP-A hTG mice, including hACE2/SP-A KO and hACE2/mSP-A (K18) mice were anesthetized using isoflurane and infected intranasally (i.n.) with 30 µl (15 µl/nose) of virus suspension containing 1×10^3 PFU of SARS-CoV-2 (delta variant) in 1X MEM. Control (SHAM) mice were inoculated with 30 µl 1X MEM. Mice were sacrificed by anesthesia and exsanguination at 6 dpi to obtain lung samples for viral load analysis by RT-qPCR and plaque assay while some mice (whole body) were fixed for 7 days in 10% neutral buffered formalin (NBF) for further analysis. We used a total of 7 mice (n=7) per group for histological, immunohistochemical and viral load analyses. After viral infection, mice were observed daily for morbidity (body weight) and mortality (survival). Mice showing >25% decrease in their initial body weight were defined as reaching experimental endpoint and euthanized.

Briefly, mock and SARS-CoV-2 infected mouse groups were anesthetized with isoflurane. After transcardial perfusion with 3 mL NBF, the lungs from SARS-CoV-2 infected groups were inflation-fixed using tracheal instillation of 1 mL NBF. Mouse whole bodies were dissected along the abdomen (n=7/group) and fixed in formalin for 7 days to completely inactivate virus before histological and immunohistochemical analysis. Lungs from a subset of mice were harvested (n= 7/group) and frozen immediately at -80 °C for further processing. The lungs were weighed and homogenized in cold PBS and then centrifuged at 21130 RCF for 5 mins and supernatants were collected for viral load analysis using RT-qPCR and plaque assay.

Lung histopathological analysis

Fixed lung tissues were embedded in paraffins as described previously (44) with some modifications. About 5 µm sections of lung tissues were cut and stained with Hematoxylin and Eosin (H&E) for light microscopic examination. Histopathological was assessed by two independent pathologists. Lung injury was scored using a 0-2 scale by counting neutrophils in the alveolar space, neutrophils in the interstitial space, hyaline membranes, proteinaceous debris filling the airspaces, and alveolar septal thickening as described by (63, 64).

Immunohistochemistry

Immunohistochemistry was analyzed as previously described by (44), with some modifications. Sections were deparaffinized in an oven at 60°C for 1 h and rehydrated sequentially with 100%, 95%, 80%, 70% and 50% ethanol. Sections were rinsed 2 times in deionized water and epitope retrieval was carried out by boiling in 10 mM citrate (pH 6.0) for 9 mins followed by cooling for 20 mins at room temperature. Nonspecific background staining was blocked with 10% BSA in PBS for 1 h at room temperature before incubating the slides at 4°C overnight with SARS-CoV-2 NP rabbit antibody (cell Signaling, #33336S; 1:100). The following day, after several washes, the sections were incubated with biotinylated goat anti-rabbit antibody for 1 h (1:200), followed by ABC/HRP complex (Vectastain ABC kit, peroxidase rat IgG PK-4004, and peroxidase rabbit IgG PK-4001; Vector Laboratories). Staining was visualized using 3'3-diaminobenzidine (DAB) (SK-4100; Vector Laboratories) for 3-5 mins and counterstained with hematoxylin (H-3404-100) (QS counterstain). Images were acquired using Nikon Eclipse TE2000-U microscope (Nikon Corporation, Tokyo, Japan).

ELISA assay

Polystyrene microtiter plates were coated with 1 µg/ml recombinant SARS-CoV-2 spike protein produced in HEK293T cells (10549-CV-100, R&D Systems and Biotech, NE, MN, USA) while some plates were coated with 50 ng/ml SARS-CoV-2 S protein

RBD or Biotinylated hACE2 (0.2 µg/ml) (EP-105; AcroBiosystems, Newark, USA) overnight at 4°C in sodium carbonate buffer (pH 9.6). The S protein has mutations that ensure its prefusion conformation. After coating, the plates were washed four times with TBST (pH 7.4-7.6) and blocked with 3% BSA diluted in TBS buffer for 1:30 mins at room temperature (RT). Then we added a series of two-fold dilutions of purified human SP-A (0-10 µg/ml, 100µl/well) in TBST containing either 5 mM $CaCl_2$ (Sigma-Aldrich, Saint Louis, MO, USA) or 10 mM EDTA (Sigma-Aldrich) and incubated at room temperature for 1 h. The wells were washed 4 times and incubated with SP-A IgG polyclonal antibody (1:1000) at room temperature for 1 h with slight shaking and SP-A-S protein or SP-A-RBD complexes were detected by adding HRP-conjugated Goat Anti-rabbit IgG (1:2000, Bio-rad, Hercules, USA) for an additional 1 h. The absorbance (450 nm) of individual wells was quantified using a spectrophotometer (Multiscan Ascent, Labsystem; Fisher Scientific, NH, USA). Experiments were carried out in duplicates from three independent experiments.

Competition assay

SP-A (10 µg/ml) was incubated simultaneously in a buffer containing 10 mM each of either maltose, mannose, galactose, or N-acetylglucosamine for 1 h in plates previously coated with either S protein (1 µg/ml) or RBD (50 ng/ml, VANC00B, R&D Systems). As a control, SP-A was incubated in a 5 mM $CaCl_2$-containing buffer without sugars. In another experiment, SP-A (10 µg/ml) was simultaneously incubated with 10 µg/ml biotinylated ACE2 in wells previously immobilized with SARS-CoV-2 RBD. Bound SP-A-S protein and/or RBD was detected with SP-A IgG polyclonal antibody (1:1000) and bound biotinylated ACE2 and RBD in the presence or absence of SP-A was detected by incubating with Streptavidin-HRP (VANC00B, R&D Systems) for 1 h at room temperature and developed as described above. All analyses were carried out in duplicate (n=3).

Pseudotyped virus entry assay in the presence of human SP-A

HEK293T-ACE2+TMPRSS2 and A549-ACE2 cells were seeded in 24-well plates to obtain confluency after a 24 h culture. Luciferase- and GFP-tagged SARS-CoV-2 pseudotyped viral particles (MOI: 5; with wildtype (WT) S protein on their surface) were pre-incubated with varying concentrations of SP-A (0 to 50 µg/ml) in 1X MEM containing 5mM $CaCl_2$ buffer for 1 h at RT. Cells were washed with 1X MEM and virus-SP-A mixture inoculated onto confluent cell monolayers and incubated at 37°C for another 2 h in a 5% CO_2 incubator. Following this, the virus-protein mix was removed and fresh medium containing 2% FBS in DMEM (500 µl/well) was added to the cells and incubated at 37°C for another 48 h. To measure luciferase intensity in cells, the cells were washed gently with sterile PBS and lysed by incubating in cell culture lysis buffer for 15 mins at room temperature with slight shaking, and Firefly luciferase activity (RLU) was measured using Luciferase Assay System (E1500 kit, Promega, Madison, WI, USA). For GFP expression analysis, cells were mounted on coverslips and GFP intensity in the cells was observed by Nikon Eclipse TE2000-U microscope (Nikon Corporation, Tokyo, Japan), and GFP-expressing cells were quantified using the Image J software.

SARS-CoV-2 (delta variant) binding, entry, and infectivity assays in the presence of human SP-A

Binding assays was performed by pre-incubating infectious SARS-CoV-2 (B.1.617.2) with human SP-A for 1 h before inoculating pre-chilled A549-ACE2 cells with virus/protein mixture at 4°C for 2 h to allow virus binding to the cell surface. The cells were washed four times with cold PBS to remove unbound viral particles. Total RNA was isolated, and the amount of virus on cells was quantified by RT-qPCR. For entry assays, after 2 h incubation of SP-A + virus mixture at 4°C, the cells were washed, and fresh media was added and shifted to 37°C for 1 h to allow virus entry into cells. Then the cells were washed and treated with proteinase K (1 mg/ml) to remove attached viral particles on the cell surface and the amount of internalized viral particles was quantified by RT-qPCR. To further assess the role of SP-A in SARS-CoV-2 entry and infectivity, we pre-incubated virus with SP-A (0 to 50 µg/ml) for 1 h before inoculating confluent A549-ACE2 cells with the virus + protein mixture for 2 h at 37°C (MOI= 0.05), unbound virus was washed, and fresh growth media added, and cells incubated at 37°C and cells and supernatant collected at 4 h and 24 hpi and viral RNA, protein and titer in cells and supernatant analyzed.

Plaque assay

The potential antiviral activity of human SP-A against SARS-CoV-2 infectivity *in vitro* and *in vivo* was detected by plaque assay in Vero E6 cells. Viral titer was quantified using supernatants from SARS-CoV-2 infected lung homogenates. *In vitro*, viral titer was quantified in 24 h cell culture media from A549-ACE2 cells inoculated with SP-A + SARS-CoV-2 as previously described (65). Briefly, Confluent monolayers of Vero E6 in 24-well plates were infected with 10-fold serial dilutions of supernatants from each group at the indicated concentrations of SP-A (see results). The cells were cultured for 1 h with intermittent rocking. The unbound virus was removed and overlayed with 2% methylcellulose and cultured for another 72 h. Upon the development of plaques, cells were fixed with 10% formalin for 1 h and stained with 0.05% (w/v) crystal violet in 20% methanol and plaques were counted.

Immunoblotting analysis

Cells were lysed with RIPA buffer (ThermoFisher Scientific, Rockford, IL) containing a cocktail of protease and phosphatase inhibitors (Roche, Indianapolis, IN). Total protein in cell lysates

obtained at 4 hpi (to assess SP-A's role in SARS-CoV-2 entry) and 24 hpi (to elucidate the effect of SP-A on viral infectivity) was determined using the BCA protein assay kit (ThermoFisher Scientific). Five micrograms of total protein were resolved by SDS-PAGE on a 10% gel under reducing conditions and transferred to PVDF membranes (Bio-Rad). The blots were blocked in TBS containing 5% non-fat milk for 30 mins and incubated with SARS-CoV-2 nucleocapsid protein antibody (1:1000, NB100-56576, Novus Biological, CO, USA) overnight at 4°C. As a loading control, blots were stripped and re-probed with β-actin (1:1000, ab-16039, Abcam, MA, USA). Subsequently, the membranes were incubated with goat anti-rabbit IgG HRP-conjugated secondary antibody (Bio-Rad) and developed using ECL Western Blotting Substrate (ThermoFisher Scientific).

Real-time quantitative PCR

Total RNA was isolated from homogenized lung tissues and from cell lysates using the Quick-RNA extraction miniprep kit (# R1055 Zymo Research, CA, USA) following the manufacturer's instructions and RNA concentration was determined by the nanodrop machine (ThermoFisher Scientific). Real-time RT-qPCR was performed using the AB StepOnePlus Detection System and the one-step kit RT-PCR Master Mix Reagents (#64471423, Biorad). Reaction mixtures were prepared according to the manufacturer's instructions. In brief, purified RNA (30 to 100 ng) was added into a 20 µl total volume of real-time PCR mix buffer containing forward/reverse primer pairs (forward, AGCCTCTTCTCGTTCCTCATCAC; reverse, CCGCCATTGCCAGCCATTC; each 500 nM) targeting SARS-CoV-2 N1 gene and a probe (250 nM, FAM) and other reagents provided by the manufacturer. The one-step q-RTPCR was carried out through one cycle of reverse transcription at 55°C for 10 mins followed by 40 cycles of amplification at 95°C for 3 mins, 95°C for 15 s, and 55°C for 1 min. The data from *in vitro* experiments were analyzed as fold change in CT values compared to SP-A untreated samples using the $2^{-\delta\delta Ct}$ method. SARS-CoV-2 copy numbers in lung tissues was quantified using SARS-CoV-2 RNA standards to enable the determination of copy number of at least 10 copies per reaction as described by Wrinkler et al. (66).

Determination of total protein and SP-A levels in human saliva specimens

Saliva samples from 40 hospitalized COVID-19 patients and 12 healthy individuals were collected following SUNY Upstate Medical University IRB approval (IRB protocol # 2020-E) and SP-A level was assessed by ELISA as previously described (67). First, the total protein concentration of the individual saliva samples was analyzed using micro-BCA method (26). Following this, 5 µg/ml of individual saliva samples and purified human SP-A as a standard (0 to 0.05 µg/ml) were coated overnight on microtiter wells. Subsequently, the SP-A level was determined by measuring the absorbance as described (67). All analyses were carried out in triplicate in three independent experiments.

Statistical analysis

All experimental data are presented as mean ± standard error and statistically analyzed using GraphPad Prism 8.0 (GraphPad Software, San Diego, CA, USA). Comparisons between two independent groups were performed using Student's *t*-test or multiple groups using one-way ANOVA. The survival analysis of mice in this study was performed with Kaplan-Meyer survival curves and evaluated statistically by the log-rank test. Shapiro-Wilk test was performed to determine normality and to evaluate the distribution of our data. Data were considered statistically significant when $P<0.05$.

Data availability statement

The original contributions presented in the study are included in the article/Supplementary Material. Further inquiries can be directed to the corresponding author.

Ethics statement

The studies involving humans were approved by SUNY Upstate Medical University IRB committee. The studies were conducted in accordance with the local legislation and institutional requirements. Written informed consent for participation in this study was provided by the participants' legal guardians/next of kin. The animal study was approved by SUNY Upstate Medical University IACUC. The study was conducted in accordance with the local legislation and institutional requirements.

Author contributions

IJ: Conceptualization, Formal analysis, Investigation, Methodology, Visualization, Writing – original draft, Writing – review & editing. AG: Formal analysis, Methodology, Writing – original draft. WX: Methodology, Writing – original draft. ER: Methodology, Writing – original draft. BN: Methodology, Writing – original draft. ST: Conceptualization, Methodology, Writing – original draft. HJ: Conceptualization, Resources, Writing – original draft, Methodology. GW: Formal analysis, Funding acquisition, Methodology, Project administration, Resources, Supervision, Writing – original draft, Writing – review & editing, Conceptualization.

Funding

The author(s) declare financial support was received for the research, authorship, and/or publication of this article. This work was supported by NIH R01HL136706, R21AI171574, the NSF research award (1722630), and the Richard and Jean Clark Pediatric Research Fund (to GW), and by the NIH 1R21AI14932101, 3R21AI149321-01S1, 1R01AI148446-01A1 (to HJ).

Acknowledgments

The authors thank all COVID-19 patients and healthy individuals who kindly provided saliva specimens used for this study. We would like to appreciate Dr. Joanna Floros for her generous support and encouragements for this project, Dr. Gary Chan for his experimental suggestions and Mr. Reuben Onwe for his critical reading and editing. We thank the staff of SUNY Upstate Pathology Research Core for providing histological services. A549-ACE2 (human lung adenocarcinoma epithelial cell overexpressing human ACE2) and Vero E6 cells were obtained from BEI Resources, NIAID, NIH.

Conflict of interest

The authors declare that the research was conducted in the absence of any commercial or financial relationships that could be construed as a potential conflict of interest.

The author(s) declared that they were an editorial board member of Frontiers, at the time of submission. This had no impact on the peer review process and the final decision.

Publisher's note

All claims expressed in this article are solely those of the authors and do not necessarily represent those of their affiliated organizations, or those of the publisher, the editors and the reviewers. Any product that may be evaluated in this article, or claim that may be made by its manufacturer, is not guaranteed or endorsed by the publisher.

Supplementary material

The Supplementary Material for this article can be found online at: https://www.frontiersin.org/articles/10.3389/fimmu.2024.1370511/full#supplementary-material

References

1. Center, C.-M.-J.H.C.R. (2023). Available online at: https://coronavirus.jhu.edu/map.html.

2. Huang C, Wang Y, Li X, Ren L, Zhao J, Hu Y, et al. Clinical features of patients infected with 2019 novel coronavirus in Wuhan, China. *Lancet*. (2020) 395:497–506. doi: 10.1016/S0140-6736(20)30183-5

3. V'Kovski P, Kratzel A, Steiner S, Stalder H, Thiel V. Coronavirus biology and replication: implications for SARS-CoV-2. *Nat Rev Microbiol*. (2021) 19:155–70. doi: 10.1038/s41579-020-00468-6

4. Xu H, Zhong L, Deng J, Peng J, Dan H, Zeng X, et al. High expression of ACE2 receptor of 2019-nCoV on the epithelial cells of oral mucosa. *Int J Oral Sci*. (2020) 12. doi: 10.1038/s41368-020-0074-x

5. Casalino L, Gaieb Z, Goldsmith JA, Hjorth CK, Dommer AC, Harbison AM, et al. Beyond shielding: the roles of glycans in the SARS-coV-2 spike protein. *ACS Cent Sci*. (2020) 6:1722–34. doi: 10.1021/acscentsci.0c01056

6. Grant OC, Montgomery D, Ito K, Woods RJ. Analysis of the SARS-CoV-2 spike protein glycan shield reveals implications for immune recognition. *Sci Rep*. (2020) 10:1–18. doi: 10.1038/s41598-020-71748-7

7. Watson A, Madsen J, Clark HW. SP-A and SP-D: dual functioning immune molecules with antiviral and immunomodulatory properties. *Front Immunol*. (2021) 11. doi: 10.3389/fimmu.2020.622598

8. Watson A, Phipps MJS, Clark HW, Skylaris CK, Madsen J. Surfactant proteins A and D: Trimerized innate immunity proteins with an affinity for viral fusion proteins. *J Innate Immun*. (2018) 11:13–28. doi: 10.1159/000492974

9. Ghildyal R, Hartley C, Varrasso A, Meanger J, Voelker DR, Anders EM, et al. Surfactant protein A binds to the fusion glycoprotein of respiratory syncytial virus and neutralizes virion infectivity. *J Infect Dis*. (1999) 180:2009–13. doi: 10.1086/315134

10. Funk CJ, Wang J, Ito Y, Travanty EA, Voelker DR, Holmes KV, et al. Infection of human alveolar macrophages by human coronavirus strain 229E. *J Gen Virol*. (2012) 93:494–503. doi: 10.1099/vir.0.038414-0

11. Benne CA, Kraaijeveld CA, van Strijp JA, Brouwer E, Harmsen M, Verhoef J, et al. Interactions of surfactant protein a with influenza a viruses: Binding and neutralization. *J Infect Dis*. (1995) 171:335–41. doi: 10.1093/infdis/171.2.335

12. Gaiha GD, Dong T, Palaniyar N, Mitchell DA, Reid KB, Clark HW. Surfactant protein A binds to HIV and inhibits direct infection of CD4+Cells, but enhances dendritic cell-mediated viral transfer. *J Immunol*. (2008) 181:601–9. doi: 10.4049/jimmunol.181.1.601

13. Hsieh MH, Beirag N, Murugaiah V, Chou Y-C, Kuo W-S, Kao H-F, et al. Human surfactant protein D binds spike protein and acts as an entry inhibitor of SARS-coV-2 pseudotyped viral particles. *Front Immunol*. (2021) 12:1–11. doi: 10.3389/fimmu.2021.641360

14. Madan T, Biswas B, Varghese PM, Subedi R, Pandit H, Idicula-Thomas S, et al. A recombinant fragment of human surfactant protein D binds spike protein and inhibits infectivity and replication of SARS-coV-2 in clinical samples. *Am J Respir Cell Mol Biol*. (2021) 65:41–53. doi: 10.1165/rcmb.2021-0005OC

15. Kase T, Suzuki Y, Kawai T, Sakamoto T, Ohtani K, Eda S, et al. Human mannan-binding lectin inhibits the infection of influenza A virus without complement. *Immunology*. (1999) 97:385–92. doi: 10.1046/j.1365-2567.1999.00781.x

16. Stravalaci M, Pagani I, Paraboschi EM, Pedotti M, Doni A, Scavello F, et al. Recognition and inhibition of SARS-CoV-2 by humoral innate immunity pattern recognition molecules. *Nat Immunol*. (2022) 23:275–86. doi: 10.1038/s41590-021-01114-w

17. Aramyan S, McGregor K, Sandeep S, Haczku A. SP-A binding to the SARS-CoV-2 spike protein using hybrid quantum and classical in silico modeling and molecular pruning by Quantum Approximate Optimization Algorithm (QAOA) Based MaxCut with ZDOCK. *Front Immunol*. (2022) 13:945317. doi: 10.3389/fimmu.2022.945317

18. LeVine AM, Gwozdz J, Stark J, Bruno M, Whitsett J, Korfhagen T. Surfactant protein-A enhances respiratory syncytial virus clearance *in vivo*. *J Clin Invest*. (1999) 103:1015–21. doi: 10.1172/JCI5849

19. Li G, Siddiqui J, Hendry M, Akiyama J, Edmondson J, Brown C, et al. Surfactant protein-A–deficient mice display an exaggerated early inflammatory response to a beta-resistant strain of influenza A virus. *Am J Respir Cell Mol Biol*. (2002) 26:277–82. doi: 10.1165/ajrcmb.26.3.4584

20. Silveyra P, Floros J. Genetic variant associations of human SP-A and SP-D with acute and chronic lung injury. *Front Biosci (Landmark Ed)*. (2012) 17:407–29. doi: 10.2741/3935

21. Altmann DM, Boyton RJ, Beale R. Immunity to SARS-CoV-2 variants of concern. *Science*. (2021) 371:1103–4. doi: 10.1126/science.abg7404

22. Planas D, Veyer D, Baidaliuk A, Staropoli I, Guivel-Benhassine F, Rajah MM, et al. Reduced sensitivity of SARS-CoV-2 variant Delta to antibody neutralization. *Nature*. (2021) 596:276–80. doi: 10.1038/s41586-021-03777-9

23. Meganck RM, Baric RS. Developing therapeutic approaches for twenty-first-century emerging infectious viral diseases. *Nat Med*. (2021) 27:401–10. doi: 10.1038/s41591-021-01282-0

24. Al-Qahtani AA, Murugaiah V, Bashir HA, Pathan AA, Abozaid SM, Makarov E, et al. Full-length human surfactant protein A inhibits influenza A virus infection of A549 lung epithelial cells: A recombinant form containing neck and lectin domains promotes infectivity. *Immunobiology*. (2019) 224:408–18. doi: 10.1016/j.imbio.2019.02.006

25. Shajahan A, Supeker NT, Gleinich AS, Azadi P. Deducing the N- and O-glycosylation profile of the spike protein of novel coronavirus SARS-CoV-2. *Glycobiology*. (2020) 30:981–988s. doi: 10.1093/glycob/cwaa042

26. Du J, Abdel-Razek O, Shi Q, Hu F, Ding G, Cooney RN, et al. Surfactant protein D attenuates acute lung and kidney injuries in pneumonia-induced sepsis through modulating apoptosis, inflammation and NF-kappaB signaling. *Sci Rep*. (2018) 8:15393. doi: 10.1038/s41598-018-33828-7

27. Luporini RL, Rodolpho JMA, Kubota LT, Martin ACBM, Cominetti MR, Anibal FF, et al. IL-6 and IL-10 are associated with disease severity and higher comorbidity in adults with COVID-19. *Cytokine*. (2021) 143:155507. doi: 10.1016/j.cyto.2021.155507

28. Wang J, Yang X, Li Y, Huang JA, Jiang J, Su N. Specific cytokines in the inflammatory cytokine storm of patients with COVID-19-associated acute respiratory distress syndrome and extrapulmonary multiple-organ dysfunction. *Virol J*. (2021) 18:117. doi: 10.1186/s12985-021-01588-y

29. Schousboe P, Ronit A, Nielsen HB, Benfield T, Wiese L, Scoutaris N, et al. Reduced levels of pulmonary surfactant in COVID-19 ARDS. *Sci Rep*. (2022) 12:4040. doi: 10.1038/s41598-022-07944-4

30. Tong M, Xiong Y, Zhu C, Xu H, Zheng Q, Jiang Y, et al. Serum surfactant protein D in COVID-19 is elevated and correlated with disease severity. *BMC Infect Dis*. (2021) 21:737. doi: 10.1186/s12879-021-06447-3

31. Ip WK, Chan KH, Law HK, Tso GH, Kong EK, Wong WH, et al. Mannose-binding lectin in severe acute respiratory syndrome coronavirus infection. *J Infect Dis*. (2005) 191:1697–704. doi: 10.1086/429631

32. Salvioni L, Testa F, Sulejmani A, Dominici R, Leoni V, Pepe F, et al. Giorgio Vittadini, *Surfactant protein D (SP-D) as a biomarker of SARS-CoV-2 infection*. *Clinica Chimi Acta*. (2022) 537:140–5. doi: 10.1016/j.cca.2022.10.013

33. Kerget B, Kerget F, Koçak AO, Kızıltunç A, Araz Ö, Uçar EY, et al. Are serum interleukin 6 and surfactant protein D levels associated with the clinical course of COVID-19? *Lung*. (2020) 198:777–84. doi: 10.1007/s00408-020-00393-8

34. Chitalia VC, Munawar AH. A painful lesson from the COVID-19 pandemic: the need for broad-spectrum, host-directed antivirals. *J Trans Med*. (2020) 18:309. doi: 10.1186/s12967-020-02476-9

35. Carter A, Mitchell KR, O'Keefe BR. Antiviral lectins: Selective inhibitors of viral entry. *Antiviral Res*. (2017) 142:37–54. doi: 10.1016/j.antiviral.2017.03.007

36. Leth-Larsen R, Zhong F, Chow VT, Holmskov U, Lu J. The SARS coronavirus spike glycoprotein is selectively recognized by lung surfactant protein D and activates macrophages. *Immunobiology*. (2007) 212:201–11. doi: 10.1016/j.imbio.2006.12.001

37. Mlcochova P, Kemp SA, Dhar MS, Papa G, Meng B, Ferreira IATM, et al. SARS-CoV-2 B.1.617.2 Delta variant replication and immune evasion. *Nature*. (2021) 599:114–9. doi: 10.1038/s41586-021-03944-y

38. Puhach O, Adea K, Hulo N, Sattonnet P, Genecand C, Iten A, et al. Infectious viral load in unvaccinated and vaccinated individuals infected with ancestral, Delta and Omicron SARS-CoV-2. *Nat Med*. (2022) 28:1491–500. doi: 10.1038/s541591-022-018160

39. Zhao H, To KK, Lam H, Zhang C, Peng Z, Meng X, et al. A trifunctional peptide broadly inhibits SARS-CoV-2 Delta and Omicron variants in hamsters. *Cell Discov*. (2022) 8:62. doi: 10.1038/s41421-022-00428-9

40. Ogando NS, Dalebout TJ, Zevenhoven-Dobbe JC, Limpens RWAL, van der Meer Y, Caly L, et al. SARS-coronavirus-2 replication in Vero E6 cells: replication kinetics, rapid adaptation and cytopathology. *J Gen Virol*. (2020) 101:925–40. doi: 10.1099/jgv.0.001453

41. Zhou Y, Lu K, Pfefferle S, Bertram S, Glowacka I, Drosten C, et al. A single asparagine-linked glycosylation site of the severe acuteRespiratory syndrome coronavirus spike glycoprotein facilitatesInhibition by mannose-binding lectin through multiple mechanisms. *J Virol*. (2010) 84:8753–64. doi: 10.1128/JVI.00554-10

42. Li L, Zheng Q, Zhang Y, Li P, Fu Y, Hou J, et al. Antiviral activity of recombinant porcine surfactant protein A against porcine reproductive and respiratory syndrome virus in vitro. *Arch Virol*. (2016) 161:1883–90. doi: 10.1007/s00705-016-2838-3

43. Juan Li MPM. Functional analysis of porcine reproductive and respiratory syndrome virus N-glycans in infection of permissive cells. *Virology*. (2015) 477:82–8. doi: 10.1016/j.virol.2015.01.005

44. Oladunni FS, Park JG, Pino PA, Gonzalez O, Akhter A, Allué-Guardia A, et al. Lethality of SARS-CoV-2 infection in K18 human angiotensin-converting enzyme 2 transgenic mice. *Nat Commun*. (2020) 11:6122. doi: 10.1038/s41467-020-19891-7

45. Sanjay H, Chotirmall L, leither M, Coruh B, Chan LLY, Joudi AM, et al. Update in COVID-19 2020. *Am J Respir Crit Care*. (2021) 203:1462–71. doi: 10.1164/rccm.202102-0415UP

46. Mirastschijski U, Dembinski R, Maedler K. Lung surfactant for pulmonary barrier restoration in patients with COVID-19 pneumonia. *Front Med*. (2020) 7. doi: 10.3389/fmed.2020.00254

47. Sender V, Hentrich K, Henriques-Normark B. Virus-induced changes of the respiratory tract environment promote secondary infections with streptococcus pneumoniae. *Front Cell Infect Microbiol*. (2021) 11:1–16. doi: 10.3389/fcimb.2021.643326

48. Floros J, Phelps DS. Is the role of lung innate immune molecules, SP-A1 and SP-A2, and of the alveolar macrophage being overlooked in COVID-19 diverse outcomes? *Pneumonia*. (2020) 33:1–5.

49. Hentschel R, Bohlin K, van Kaam A, Fuchs H, Danhaive O. Surfactant replacement therapy: from biological basis to current clinical practice. *Pediatr Res*. (2020) 88:176–83. doi: 10.1038/s41390-020-0750-8

50. Malloy JL, Veldhuizen RA, Thibodeaux BA, O'Callaghan RJ, Wright JR. Pseudomonas aeruginosa protease IV degrades surfactant proteins and inhibits surfactant host defense and biophysical functions. *Am J Physiol Lung Cell Mol Physiol*. (2005) 288:L409–18. doi: 10.1152/ajplung.00322.2004

51. Islam ABMMK, Khan MA-A-K. Lung transcriptome of a COVID-19 patient and systems biology predictions suggest impaired surfactant production which may be druggable by surfactant therapy. *Sci Rep*. (2020) 10:19395. doi: 10.1038/s41598-020-76404-8

52. Xiang Q, Feng Z, Diao B, Tu C, Qiao Q, Yang H, et al. SARS-coV-2 induces lymphocytopenia by promoting inflammation and decimates secondary lymphoid organs. *Front Immunol*. (2021) 12:1–13s. doi: 10.3389/fimmu.2021.661052

53. Lv Z, Cheng S, Le J, Huang J, Feng L, Zhang B. Clinical characteristics and co-infections of 354 hospitalized patients with COVID-19 in Wuhan, China: a retrospective cohort study. *Microbes Infect*. (2020) 22:195–9. doi: 10.1016/j.micinf.2020.05.007

54. Contou D, Claudinon A, Pajot O, Micaëlo M, Longuet Flandre P, Dubert M, et al. Bacterial and viral co-infections in patients with severe SARS-CoV-2 pneumonia admitted to a French ICU. *Ann Intensive Care*. (2020) 10:119. doi: 10.1186/s13613-020-00736-x

55. Floros J, Wang G, Mikerov AN. Genetic complexity of the human innate host defense molecules, surfactant protein A1 (SP-A1) and SP-A2 - Impact on function. *Crit Rev Eukaryotic Gene Expression*. (2009) 19:125–37. doi: 10.1615/CritRevEukarGeneExpr.v19.i2

56. Mikerov AN, White M, Hartshorn K, Wang G, Floros J. Inhibition of hemagglutination activity of influenza A viruses by SP-A1 and SP-A2 variants expressed in CHO cells. *Med Microbiol Immunol*. (2008) 197:9–12. doi: 10.1007/s00430-007-0051-4

57. Wang X, Guo X, Xin Q, Pan Y, Hu Y, Li J, et al. Neutralizing antibodies responses to SARS-coV-2 in COVID-19 inpatients and convalescent patients. *Clin Infect Dis*. (2020) 71:2688–94. doi: 10.1101/2020.04.15.20065623

58. Tate MD, Brooks AG, Reading PC. Specific sites ofN-linked glycosylation on the hemagglutinin of H1N1 subtype influenza A virus determine sensitivity to inhibitors of the innate immune system and virulence in mice. *J Immunol*. (2011) 187:1884–94. doi: 10.4049/jimmunol.1100295

59. NikoLaos M, Nikolaidis MRW, Allen K, Tripathi S, Qi L, McDonald B, et al. Hartshorn, *Mutations flanking the carbohydrate binding site of surfactant protein D confer antiviral activity for pandemic influenza A viruses*. *Am J Physiol Lung Cell Mol Physiol*. (2014) 306:1036–44. doi: 10.1152/ajplung.00035.2014

60. Wang G, Phelps DS, Umstead TM, Floros J. Human SP-A protein variants derived from one or both genes stimulate TNF-α production in the THP-1 cell line. *Am J Physiol - Lung Cell Mol Physiol*. (2000) 278:946–54. doi: 10.1152/ajplung.2000.278.5.L946

61. Johnson MC, Lyddon TD, Suarez R, Salcedo B, LePique M, Graham M, et al. Optimized pseudotyping conditions for the SARS-COV-2 spike glycoprotein. *J Virol*. (2020) 94:e01062-20. doi: 10.1128/JVI.01062-20

62. Anderson CF, Wang Q, Stern D, Leonard EK, Sun B, Fergie KJ, et al. Supramolecular filaments for concurrent ACE2 docking and enzymatic activity silencing enable coronavirus capture and infection prevention. *Matter*. (2022) 6:583–604. doi: 10.1016/j.matt.2022.11.027

63. Matute-Bello G, Downey G, Moore BB, Groshong SD, Matthay MA, Slutsky AS, et al. An official American Thoracic Society workshop report: features and measurements of experimental acute lung injury in animals. *Am J Respir Cell Mol Biol*. (2011) 44:725–38. doi: 10.1165/rcmb.2009-0210ST

64. Xu Y, Ge L, Abdel-Razek O, Jain S, Liu Z, Hong Y, et al. Differential susceptibility of human sp-B genetic variants on lung injury caused by bacterial pneumonia and the effect of a chemically modified curcumin. *Shock*. (2016) 45:375–84. doi: 10.1097/SHK.0000000000000535

65. Case JB, Bailey AL, Arthur S, Rita E, Michael S. Diamond, *Growth, detection, quantification, and inactivation of SARS-CoV-2*. *Virology*. (2020) 548:39–48. doi: 10.1016/j.virol.2020.05.015

66. Winkler ES, Bailey AL, Kafai NM, Nair S, McCune BT, Yu J, et al. SARS-CoV-2 infection of human ACE2-transgenic mice causes severe lung inflammation and impaired function. *Nat Immunol*. (2020) 21:1327–35. doi: 10.1038/s41590-020-0778-2

67. Phelps DS, Umstead TM, Mejia M, Carrillo G, Pardo A, Selman M. Increased surfactant protein-A levels in patients with newly diagnosed idiopathic pulmonary fibrosis. *Chest*. (2004) 125:617–25. doi: 10.1378/chest.125.2.617